

VLSI Implementation of a Neuromorphic Spiking Pixel and Investigation of Various Focal-Plane Excitation Schemes

Amine Bermak

Abstract

In this paper we describe a Neuromorphic spiking pixel architecture allowing the conversion of the light intensity into a pulse train signal. We first describe the spiking pixel architecture and its inherent advantages such as light adaptation mechanism and linear response characteristics. Inspired from biological visual systems and the integrate and fire oscillator, different inter-pixels interaction schemes are studied and their synchronization ability are compared. The spiking pixel architecture was implemented and the functionality of the spiking pixel imager is demonstrated through experimental results.

Keywords

Spiking pixel architecture, synchronization ability, light adaptation mechanism.

I. INTRODUCTION

CMOS image sensors are being used in an increasing number of low power and low cost applications. This is mainly due to the use of standard CMOS technology which allows for the realization of image capture devices as well as image processing circuitry on a single chip [1], [2], [3]. In addition, it is expected that on-chip signal processing would allow the realization of the next generation on-chip visual systems. The latter would be equipped with intelligent processing such as detecting, recognizing and tracking complex moving objects. Biologically inspired image processing based on the spiking pixel architecture are becoming more and

Amine Bermak is with Hong Kong University of Science and Technology, Electrical and Electronic Engineering Department, Clear Water Bay, Kowloon, HK. E-mail:eebermak@ust.hk

more popular [4], [5], [6] and several versions of spiking pixel circuits have been proposed in the literature [7], [8], [9]. A straightforward approach relies on generating a pulse when the analog voltage (typically the voltage of the photodiode) reaches a given threshold voltage. For example in [10] a chain of inverters are used in order to realize a free running oscillator presenting a frequency that is proportional to the photocurrent. This last approach is known for its compactness unfortunately at the expense of higher power consumption in the inverter chain particularly critical because of the slow transition of the photodetector node. In [6] the authors specifically address the problem of power consumption by proposing a very elegant inverter structure with feedback current which is shown to significantly reduce the power consumed during the spike generation. The previously mentioned spiking pixels do offer the advantage of mimicking biological systems, however their utilization in focal plane locally interconnected structure is quite challenging as they do not integrate voltage threshold modulation [11] and do require special read-out structures typically known as Address Event Representation (AER).

In this paper, we first describe a spiking pixel architecture based on the use of an on-pixel comparator, enabling access to the threshold voltage of the oscillator, and an on-pixel counter/memory circuitry allowing local storage and avoiding the need for complex read-out structures. The pixel array is first designed and its light adaptation mechanism is demonstrated. Several excitation schemes are then simulated in which interaction between pixels is locally obtained and is mediated via the discharge speed of each spiking pixel. This model is very close to the behavior of integrate-and-fire oscillators which can be used for image segmentation when organized in a Locally Excitatory Globally Inhibitory Oscillator Network [12], [13]. The behavior of a single pixel as well as locally coupled pixels is presented in this paper. Different types of local inter-pixel interaction are studied. Section II presents the spiking pixel architecture and describes its inherent advantages. Section III describes a locally interconnected spiking pixels network that can be potentially used for image segmentation. Different local inter-pixel interaction schemes are described and their ability to perform pulse synchronization is simulated and compared. Section IV describes the VLSI implementation of the spiking pixel architecture and its experimental results. Section V discusses the obtained results.

II. SPIKING PIXEL ARCHITECTURE (SPA)

Our spiking pixel structure takes advantage of the very high level of integration in sub-micron CMOS technologies allowing us to integrate in a reasonable area the free oscillator circuit followed by an on-pixel counter/memory. This approach, even requiring higher number of transistors, enables local storage of digital data leading to the realization of Digital Pixel Sensor as well as biologically inspired analog processing. The analog output of the pixel is converted into a train of pulses coded as Pulse Frequency Modulation (PFM) signals. This approach also eliminates voltage/current domain analog processing and hence provides immunity to dynamic range reduction caused by low voltage operation in advanced sub-micron technologies.

A. Principle of operation

The spiking pixel (Fig. 1.A) is composed of a photosensitive device (photodiode P_d) with its internal capacitance C_d , a PMOS reset transistor, a feedback circuit, a comparator followed by an on-pixel counter/memory.

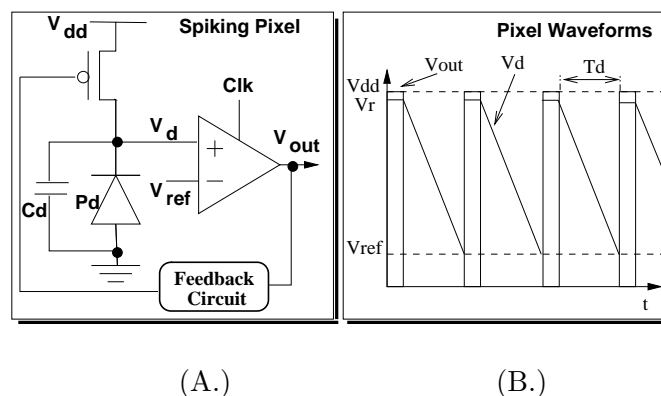


Fig. 1. (A.) Block diagram of the spiking pixel based. (B.) Waveforms of the different node of the circuit. V_d is the voltage at the sensing photodiode node, V_{out} is the output voltage of the comparator

During the reset operation, the voltage node V_d of the photodiode is reset to V_r . After the reset phase, the light falling onto the photodiode P_d discharges the internal capacitor of the photodiode C_d , resulting in a decreasing voltage V_d across the photodiode node, as shown in Fig. 1.B. Once the voltage V_d reaches a reference voltage V_{ref} , the output of the comparator (V_{out}) is switched high and a feedback circuit is used to reset the photodiode again. Fig. 1.B shows the voltage across the photodiode V_d , where T_d represents the discharge time of the capacitor from V_r to V_{ref} . Assuming that the photocurrent i_d is constant during the

oscillation process and assuming that the capacitance C_d is also constant over the range of voltages ($V_r : V_{ref}$), the discharge time T_d can then be expressed as function of the photocurrent i_d

$$T_d = \frac{(V_r - V_{ref}) \times C_d}{i_d}. \quad (1)$$

The frequency f of the voltage across the photodiode V_d is inversely proportional to T_d , expressed as

$$f \approx \frac{1}{T_d} = \frac{i_d}{k}, \quad \text{with } k = (V_r - V_{ref}) \times C_d. \quad (2)$$

The switching frequency of the comparator output V_{out} , is directly proportional to the capacitor discharge current i_d . The output of each spiking pixel is a signal which is very similar to a Pulse Frequency Modulation (PFM) scheme whereby the frequency of the train pulses is proportional to the photocurrent (Eq. (2)).

B. Pixel response linearity

The main advantage of the spiking pixel is its linear response. This feature is clearly shown through Eq. (2) where we can note that the frequency of the comparator's output signal is directly proportional to the photocurrent i_d . In addition the sensitivity of the sensor expressed by: $\frac{1}{(V_r - V_{ref}) \times C_d}$ can be set by changing the reference voltage V_{ref} . For low levels of illumination the reference voltage could be increased in order to lower the required conversion time. Fig. 2 shows the simulation results for the frequency f of the spiking pixel as function of the photocurrent i_d . The result suggests a linear response for a wide range of illuminations.

C. Light Adaptation mechanism

The spiking pixel can be used as a digital pixel sensor (DPS) with pixel level light adaptation mechanism. Adaptation to light intensity is a very important criteria for vision sensors because natural light levels can vary by over eight orders of magnitude [14]. The dynamic range of conventional CMOS imagers is mainly limited by the photodiode linear response, causing blooming to occur for typical natural scene illumination conditions. Light adaptation is simply obtained by connecting the output of the comparator to the input of a digital counter/register with an enable signal (En) provided externally. The counter is only operational during a counting period T_{cnt} , set by the external En signal. The number of impulses detected by the counter

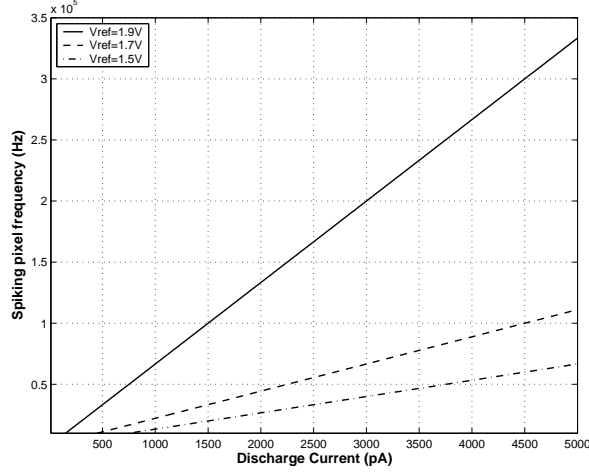


Fig. 2. Simulation results of the pixel response as function of the photocurrent for different values of the reference voltage (V_{ref}). In this simulation $V_r = 2V$ and $C = 150fF$ and the leakage current is disregarded and it is assumed that no oscillation will occur for a nil photocurrent.

is therefore given by $N_{imp} \simeq \frac{T_{cnt}}{T_d}$. By replacing T_d by its value we obtain

$$N_{imp} \simeq \frac{T_{cnt} \times i_d}{(V_r - V_{ref}) \times C_d}. \quad (3)$$

Light adaptation is therefore obtained by modulating the T_{cnt} signal according to the mean light intensity. If the sensor is being used in a scene where illumination levels result in a photocurrent varying from 0 to i_{dm} , then T_{cnt} will be modulated such that 2^n impulses resulting from DPS are counted for the maximum photocurrent i_{dm} , where n is the number of bits. By substituting $N_{imp} = 2^n$ and $i_d = i_{dm}$ in Eq. (3) we deduce the optimum T_{cnt} as

$$T_{cnt} = 2^n \times \frac{(V_r - V_{ref})}{i_{dm}} \times C_d. \quad (4)$$

According to this adaptation mechanism, when the photocurrent varies from 0 to i_{dm} , a corresponding optimum T_{cnt} can be obtained using Eq. (4). This T_{cnt} will correspond to the minimum counting time that allows the use of the pixel's full range. In other words, T_{cnt} will optimize the dynamic range as well as the conversion speed of the pixel. Longer conversion time is required for increased accuracy as well as lower photocurrent. For a given photocurrent, there exists one, and only one T_{cnt} , that optimizes both the conversion speed and the Signal to Quantization Noise Ratio (SQNR). For optimal use of the sensor, one must first estimate the maximum photocurrent and then calculate the optimum T_{cnt} (using Eq. 4) that yields

to the maximum SQNR without affecting the conversion speed. On one hand, by choosing T_{cnt} lower than the optimum value, the SQNR is decreased. On the other hand, by choosing T_{cnt} higher than the optimum value, the conversion speed is reduced without any gain in terms of SQNR performance (flat curve at about SQNR = 48dB for 8-bit conversion). Keeping T_{cnt} constant and reducing i_{dm} by half results in a 6dB loss in SQNR, which corresponds to one bit at the digital output. As a conclusion, T_{cnt} provides the possibility of inter-scene adaptation enabling the spiking pixel to operate within its full range. This last feature is usually obtained through a complex gain control amplifier integrated within the photodetector array. In our case, this is simply realized by using a digital enable signal of a conventional digital counter.

III. EXCITATION SCHEMES USING SPA

In focal plane biologically inspired image processing it is often required to implement different spatial and temporal interaction between neighboring pixels. For example, to achieve image segmentation, pixels are examined whether to be identified with neighboring pixels based on mean characteristics and spatial-relationship. As a result, pixels are grouped in the same class if a criterion of homogeneity is satisfied. It should be noticed that the architecture of spiking pixel, described in section II, acts as an oscillator with an output frequency depending on the illumination. This model presents some analogy with the integrate-and-fire oscillator which has been proven to be a good tool for image segmentation when arranged in a Local Excitation Global Inhibition Networks (LEGION) [12]. Inspired from this model, we developed a criteria of spatial homogeneity based on synchronization of adjacent spiking pixels. A criteria of homogeneity can be set by looking at the output frequency of adjacent pixels and their ability to synchronize. Two pixels that fire with equal frequencies would satisfy the homogeneity criteria.

A. Excitation and Inhibition Mechanisms

Excitation and inhibition mechanisms can also be obtained in the spiking pixel architecture by modifying the discharge curve of the pixel. Interaction between adjacent pixels is mediated via the discharge speed of each pixel, as seen in Fig. 3 for example, which shows a pair of coupled spiking pixels. Depending on the current I_{pulse} , this model can implement either excitation or inhibition operations, which are useful processes

for region-based bio-inspired segmentation. If the discharge curve is accelerated an excitation mechanism is obtained while if the discharge curve is slowed down an inhibition mechanism is obtained.

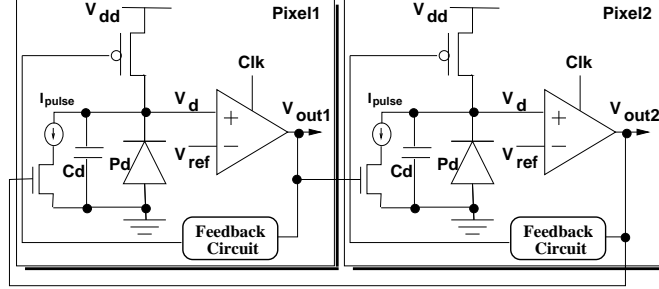


Fig. 3. Example of coupling two spiking pixels.

When the potential of one pixel on Fig. 3, drops below the reference voltage, it will generate a pulse at the comparator output and will reset the pixel. This is referred to as *firing state*. An instantaneous excitation impulse is sent to the adjacent pixel which is forced by a current impulse I_{pulse} to increase its slope. In this example, a clocked comparator is used which would only trigger for half a clock cycle. Hence, the excitation will only take place for half a cycle corresponding to a certain voltage drop ΔV which is ideally expressed as

$$\Delta V = \frac{i_{pulse}}{2 \cdot C_d \cdot f_{Clk}}. \quad (5)$$

If this voltage drop brings the node voltage of the excited pixel below the reference voltage, the excited pixel will fire as well.

The effect of coupling two pixels using a controlled current source, as represented in Fig. 3, has been simulated for different levels of illuminations and for different coupling strengths. Fig. 4(a) shows the synchronization ability of two pixels at different illuminations and excitation strengths (I_{pulse}). The z-axis represents the number of unsynchronized cycles, thus the lower this value, the faster the synchronization will occur, and hence the criteria of homogeneity is satisfied. In this example, 200 cycles were simulated for each pair of parameters (illumination and excitation strength). Pixel 1 received a constant illumination of 550 lx while the illumination of pixel 2 is varied by $\pm 18\%$ of that of pixel 1 (450 lx to 650 lx). Area A corresponds to the case where the pixels synchronize immediately because they receive exactly the same illumination. Area B corresponds to the case where the pixels are synchronized after a couple of cycles. Finally, Area C corresponds to

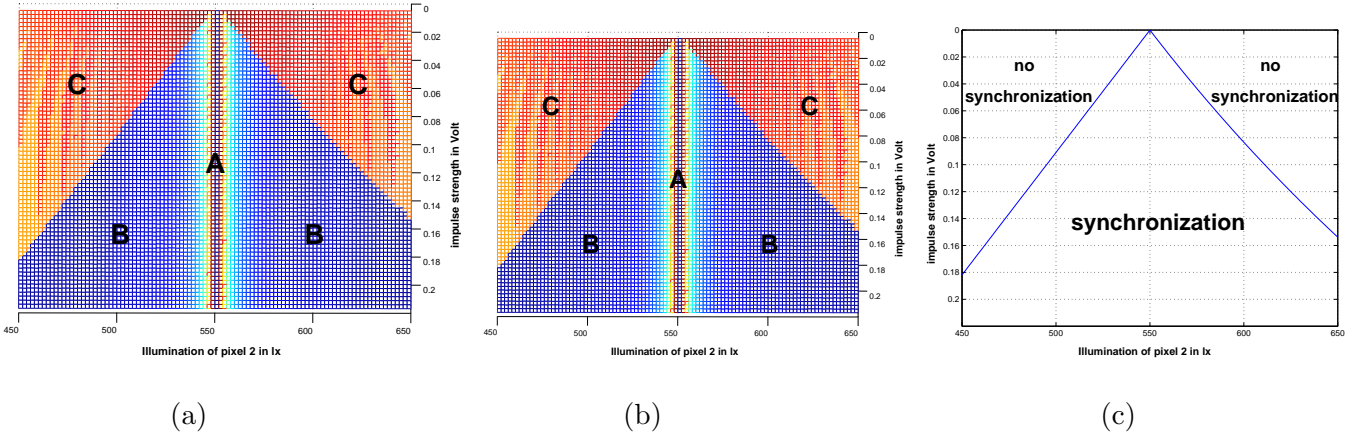


Fig. 4. (a) Synchronization ability of two pixels at different illuminations and excitation strengths. The x-axis, y-axis and z-axis represent illumination of diode 2, excitation strength and the number of unsynchronized cycles respectively. (b) Top view of the 3D-plot in (a). (c) Graph derived theoretically from Eq.(6)

the case where the pixels do not synchronize at all because the excitation strength is too weak. This happens in the case where the voltage drop ΔV due to excitation is less than the diode with the higher illumination is able to catch up in one discharging period of the slower diode. In order to achieve synchronization, the excitation pulse must cause a minimal voltage drop of:

$$\Delta V = (V_{dd} - V_{ref}) \cdot \left(1 - \frac{Il_2}{Il_1}\right) \quad (6)$$

Note that this condition allows for synchronization in one clock cycle, and even if ΔV is lower than the value derived in Eq. (6), synchronization may still be achieved. Synchronization conditions for unidirectional and two directional weakly coupled neurons have been derived previously in [15], [16].

The theoretical condition of synchronization illustrated by Eq. (6) and represented on Fig. 4(c), is in good accordance with the simulation results represented on Fig. 4(b). It should be however noticed from Fig. 4(a) that synchronization takes longer the closer the illuminations of the pixels are because the slopes differ only slightly and hence it takes more time for the synchronization to occur. This is illustrated by region A shown in both Fig. 4(a) and 4(b). This is explained by the fact that a pixel that is induced to fire will re-excite the inducing pixel at the next clock cycle. After this re-excitation process, the phase difference between the two pixels is even larger than prior to the firing state, which does not help the synchronization process. This

effect is further shown in Fig. 5(a) illustrating the phase difference between two pixels prior and after firing.

B. Improved excitation schemes

In order to resolve the re-excitation problem illustrated by Fig. 5(a), we propose the two new schemes represented on Fig. 5(b) and 5(c).

B1. Adaptive excitation strength: The oscillators in the LEGION model follow an exponential trajectory instead of the linear discharge function of our spiking pixels. This exponential behavior has an additional synchronizing effect since the excitation impulse causes a stronger impact on a pixel that is close to the threshold than on a pixel that is still far away. We can simulate this effect by adapting the excitation strength to the actual potential of the excited pixel as shown on Fig. 5(b). In this process the excitation strength is stronger the closer the adjacent pixels are to the reference voltage.

B2. Feedback controlled reference voltage: A fully different way of carrying out the excitation is to change the reference voltage of an excited pixel instead of sending a current impulse. The reference voltage of an excited pixel will be increased by a voltage corresponding to Eq. (6). Therefore a pixel that is close enough to the threshold will fire at the following clock cycle but the excitation will have no effect on a pixel that is far away from the threshold. Fig. 5(c) shows this principle.

The simulation results for a pair of coupled spiking pixels using the two improved excitation methods are shown in Fig. 6. It was found that the two methods give the same results. As it can be seen from Fig. 6, the peaks in synchronization time for very similar illuminations of the adjacent pixels are completely vanished allowing synchronization to happen for well-defined excitation strengths. The unwanted behavior illustrated by region A of Fig. 4(a) and 4(b) are eliminated. The synchronization ability of two pixels is tuned by setting the excitation strength which is represented by the feedback quantity (discharge current or reference voltage).

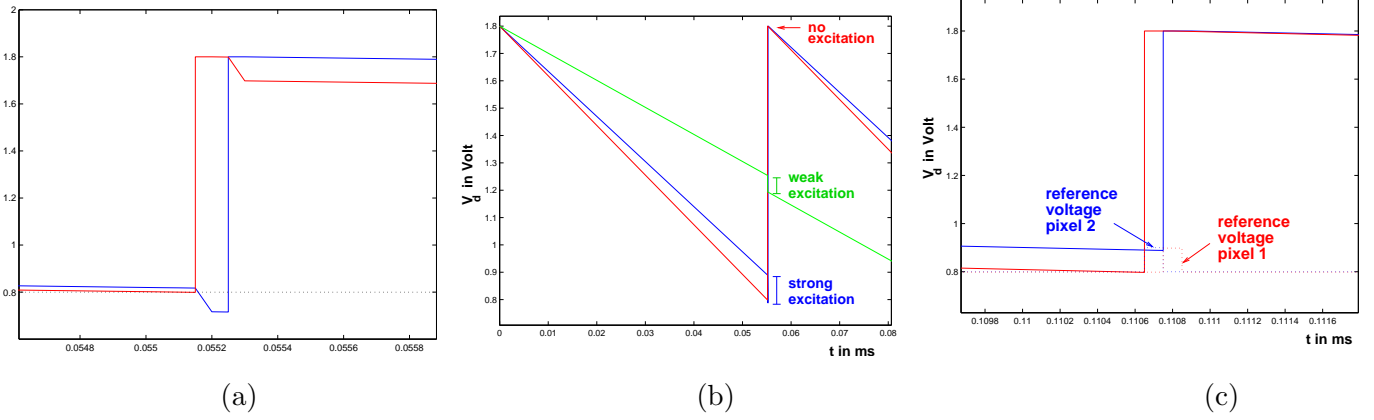


Fig. 5. (a) Synchronization of a pair of pixels using the initial scheme of feedback controlled current source. (b) Synchronization of a pair of pixels by using adaptive excitation strength process. The excitation strength is stronger the closer the adjacent pixels are to the reference voltage. (c) Synchronization of a pair of pixels by changing the reference voltage during excitation.

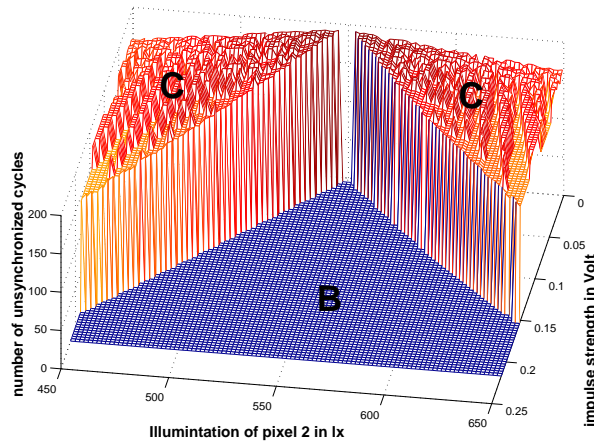


Fig. 6. Synchronization ability of two pixels at different illuminations and excitation strengths using the improved excitation methods. The x-axis, y-axis and z-axis represent illumination of diode 2, excitation strength and the number of unsynchronized cycles, respectively.

C. Simulation results

The synchronization ability of an array of pixels using the proposed schemes has also been simulated. In the proposed interaction schemes, each pixel is only connected to its four adjacent neighbors. We first validated our models using low resolution gray scale artificial images. Electrical simulation of such models for even low resolution arrays is time consuming. In order to reduce the simulation time, a Matlab model was developed and the synchronization ability of an $n \times n$ array of pixels for different illuminations was simulated.

The illumination values for an $n \times n$ array were randomly generated based on a uniform distribution of illumination between 475 lx and 525 lx. V_r and V_{ref} were set to 1.8V and 0.8V, respectively. According to Eq. (6), an excitation strength of 0.12V was chosen for the simulation. Fig. 7(a) shows the node voltages of an array of 7×7 pixels for different illuminations while Fig. 7(a') shows the counter values for each pixel within the array. Fig. 7(b) shows the results of the coupling effect using the initial excitation scheme as proposed by Fig. 3 (feedback controlled current source). We can note from Fig. 7(b) and Fig. 7(b') that the feedback controlled current source is unable to synchronize the array of pixels as it suffers from re-excitation problem discussed earlier. Fig. 7(c) shows the results of the coupling effect using the feedback controlled reference voltage as explained in Fig. 5(c). We can note from Fig. 7(c) and 7(c') that the proposed advanced excitation scheme is able to synchronize the entire array as the node voltage of all pixels are synchronized (Fig. 7(c)) and the counter values are equal for the entire array (Fig. 7(c')). An entire array of pixels can therefore be synchronized by choosing an excitation impulse according to Eq. (6). However, one must note that a system that only achieves synchrony is not very useful as it will result in information loss. The aim is to synchronize only pixels that belong to a certain object in the scene. In order to test the improved architectures proposed previously, we used several gray scale artificial images and for each image, different objects can be identified by their illumination distribution. A random noise was also added to each pixel value. Fig. 8(a) shows an example of 7×7 gray scale image containing four different shapes on a dark background while Fig. 8(a') shows the illumination distribution for each shape or object within the image.

Fig. 8(b) and 8(b') show the results of the coupling effect using the initial excitation scheme as proposed by Fig. 3 (feedback controlled current source). We can note from Fig. 8(b) and Fig. 8(b') that the feedback controlled current source is unable to synchronize pixels belonging to the same object. The scheme clearly fail to achieve any kind of segmentation. Moreover the processed image is noisier as compared to the original image. Fig. 8(c) shows the result of the coupling effect using the feedback controlled reference voltage as explained in Fig. 5(c). We can note from Fig. 8(c) and 8(c') that the proposed advanced excitation scheme is able to synchronize pixels belonging to the same shape or object. Pixels belonging to the same object have exactly the same counter value as illustrated by Fig. 8(c').

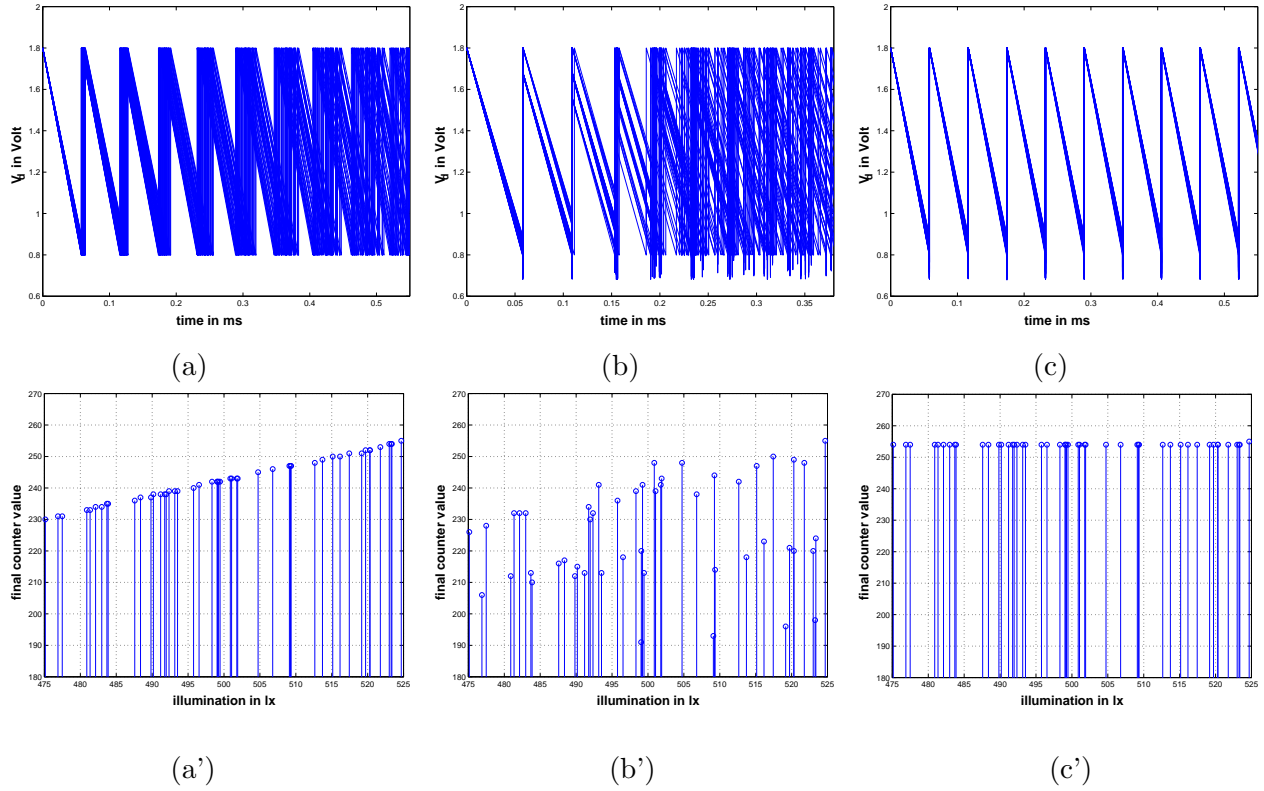


Fig. 7. (a) Synchronization of an array of pixels. (a), (b) and (c) are the node voltages of an array of 7×7 pixels for the original array, using the feedback controlled current source and using the feedback controlled reference voltage, respectively. (a'), (b') and (c') are the corresponding counter values for each pixel within the array.

The obtained results, even tested on low resolution and using simple patterns, show that simple interaction schemes can be useful and can also be incorporated at the pixel level allowing focal-plane processing. In addition, the feedback controlled reference voltage is suitable for VLSI implementation particularly for a locally interconnected network. Having access to the threshold voltage of the firing pixel is proven to be useful as it can be used to implement excitation and inhibition processes. Further improvements are to be considered if image segmentation is to be successfully implemented on real and high resolution images. These improvements include, investigating new phase coding techniques instead of frequency coding of neurons' information, as is the case in LEGION model [12], [17]. It is also important to consider in future work an efficient way to provide a global inhibition mechanism and also to consider a normalization procedure which is shown to improve the synchronization performance [12].

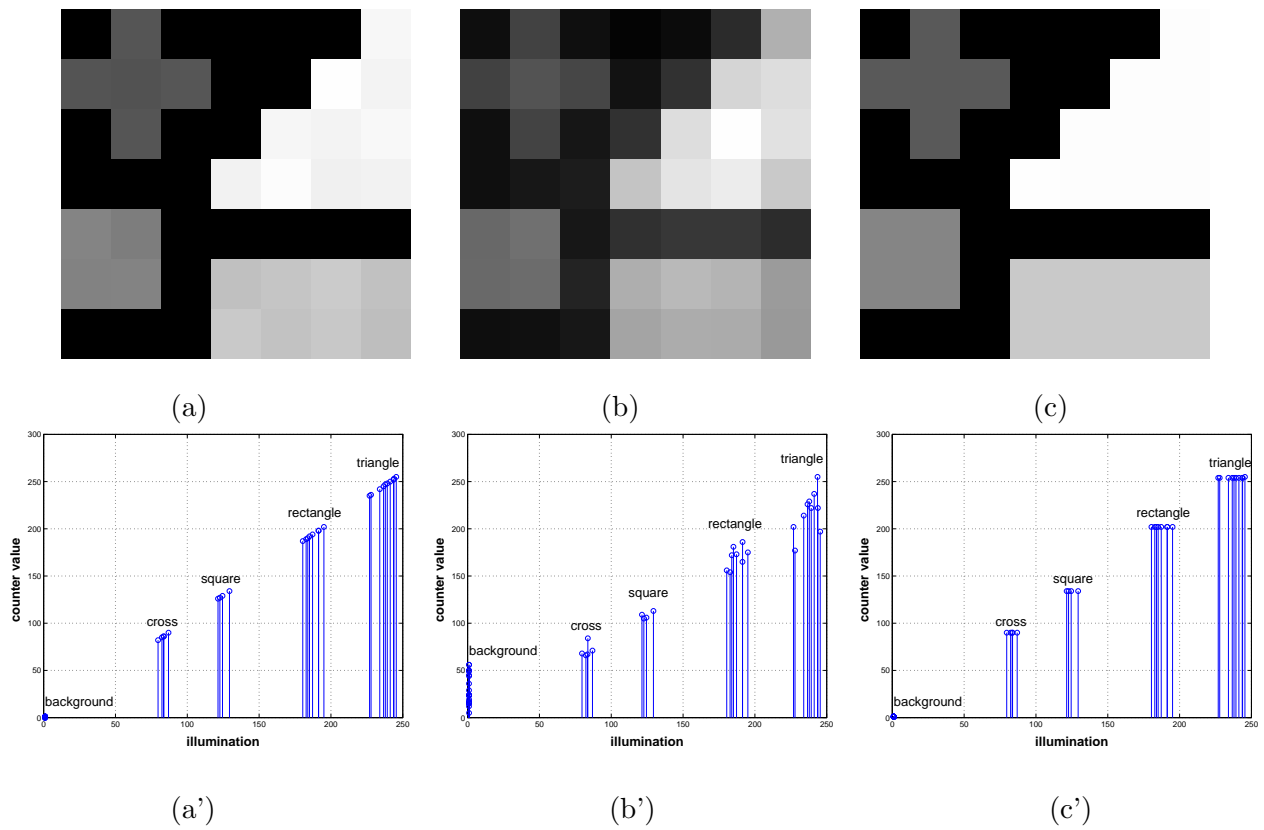


Fig. 8. (a) Image Segmentation for an array of pixels. (a) is a 7×7 gray scale image containing four different shapes on a dark background while (a') shows the counter values for each shape or object within the image. (b) is the processed image using feedback controlled current source and (b') is the corresponding counter value for each object. (c) is the processed image using feedback controlled reference voltage and (c') is the corresponding counter value for each object.

IV. VLSI IMPLEMENTATION AND EXPERIMENTAL RESULTS

The spiking pixel as well as the feedback controlled reference voltage model present the advantage of simple VLSI implementation which makes them very suitable for smart vision systems application. Fig. 9 shows the feedback controlled reference voltage model. This circuit includes a photodetector, a comparator, a set of buffers as well as a set of switches used to select the corresponding reference voltage which is feed to the comparator. When a pixel fires, it will provide a self-reset pulse with a duration equal to the delay of the chain buffers. At the same time, the state of the switch of inter-connected pixels will be changed allowing to increase the reference voltage of these pixels, hence realizing the excitation process. If the excited pixel fires, it will not initiate re-excitation as the voltage node of the inducing pixel is close to its reset level.

The controlled reference voltage model, even proven to be effective, requires reliable distribution of multiple

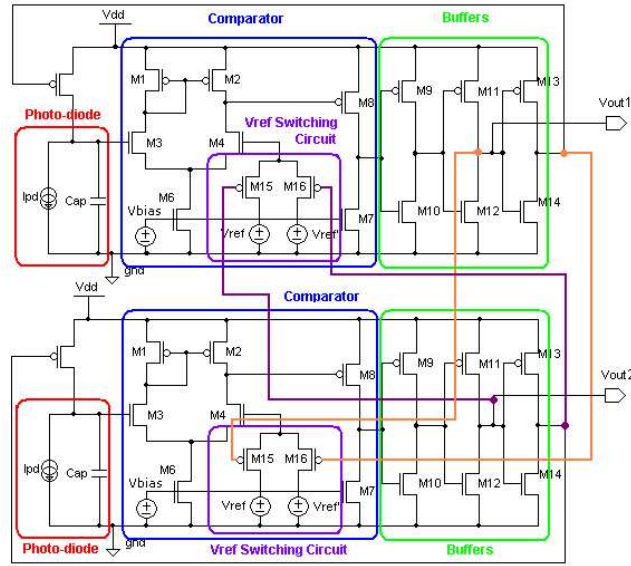


Fig. 9. Schematic circuit of the feedback controlled reference voltage. The circuit shows two inter-connected pixels.

reference voltages (at least two reference voltages), which is quite hard to achieve within a large VLSI chip. In order to evaluate the sensitivity of our approach to the reference voltage distribution, we have simulated the effect of the reference voltage mismatch on the synchronization ability of two pixels. A variation on V_{ref} of $\pm 5\%$ was introduced and its effect on the synchronization ability was simulated. The results are shown in Fig. 10. It is clear from this figure that the mismatch will introduce a deviation from the initial boundary between synchronized and unsynchronized areas. A bandgap circuit is therefore required in our approach in order to effectively distribute multiple reference voltages within the chip.

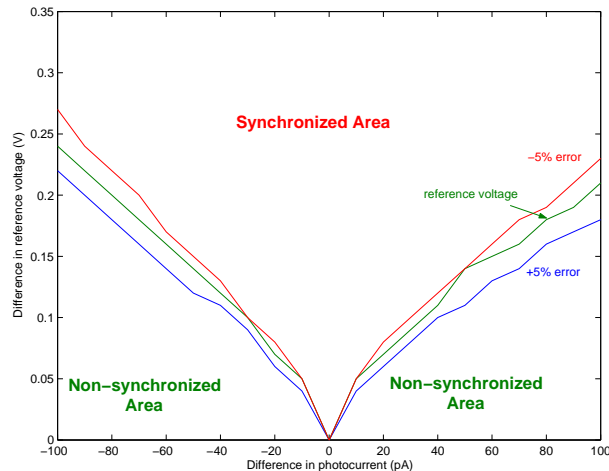


Fig. 10. V_{ref} mismatch analysis.

A prototype testing the spiking pixel architecture has been implemented in $0.25\mu\text{m}$ CMOS technology. Fig. 11 shows the layout of the spiking pixel occupying a silicon area of $45 \times 45\mu\text{m}^2$ with a fill factor of 23%. An

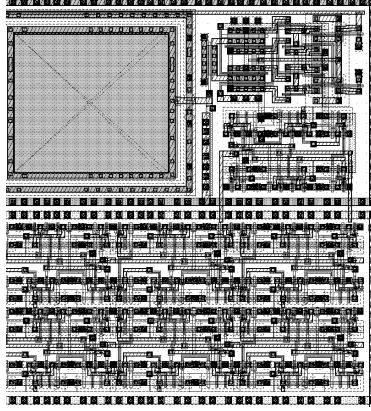


Fig. 11. Layout of the spiking pixel. It occupies an area of $45 \times 45\mu\text{m}^2$ with a fill-factor of 23%.

experimental setup was used including the sensor mounted on a PCB board and a data acquisition board for the sensor' data acquisition. The light intensity was controlled using a light source which is connected to an optical sphere in order to obtain uniform illumination. The array was operated under different illumination levels in order to test the light adaptation mechanism introduced in section II.

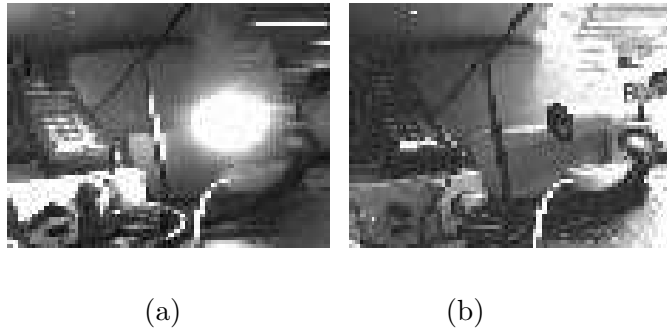


Fig. 12. Sample images from the spiking pixel array obtained for $T_{cnt} = 120\text{ms}$ and $T_{cnt} = 830\text{ms}$ with a 40W Lamp switched On and Off, respectively.

Fig. 12(a) and 12(b) show two sample images acquired from the spiking pixel array obtained at $T_{cnt} = 120\text{ms}$ and $T_{cnt} = 830\text{ms}$, with a 40W Lamp switched On and Off, respectively. Fig. 13 shows experimentally measured frequencies as function of illumination, which reflects the linearity advantage of the spiking pixel. Dark current was also estimated by blocking all light from the array and measuring the average firing rate recorded at 32s. One should note that the speed of the imager depends on the illumination level, which can be

slow for low illumination levels (few hundred ms for typical office light). However, it is important to mention that focal plane image processing will then be performed at the acquisition speed, which would make this architecture attractive.

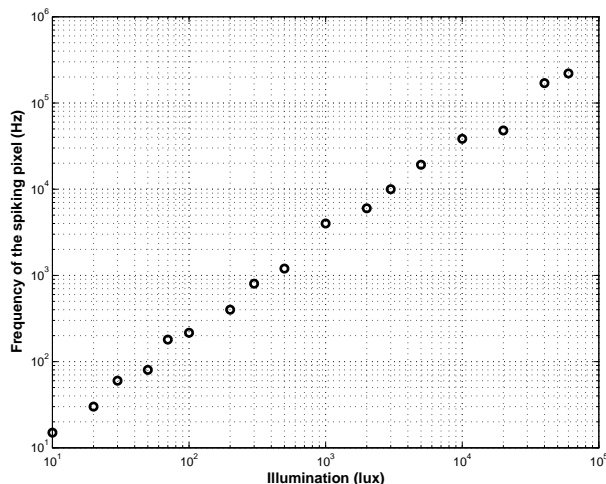


Fig. 13. Experimentally measured frequencies as function of illumination.

V. CONCLUSION

In this paper a spiking pixel architecture together with its inherent advantages such as linear response and built-in light adaptation mechanism is presented. The spiking pixel array was tested and its light adaptation mechanism was proven to be functional. Different excitation schemes for locally coupled pixels were simulated. Improved models have been proposed in order to overcome the re-excitation problem found in the feedback controlled current source scheme. The ability of the proposed models to perform inter-pixels synchronization has been evaluated. The obtained results, even tested on low resolution and using simple patterns, show that simple interaction schemes can be useful and can also be incorporated at the pixel level allowing focal-plane processing. Further work is being conducted in order to improve the proposed techniques.

ACKNOWLEDGMENTS

The work described in this paper was partly supported by a Grant from the Research Grant Council of Hong Kong, Grant ref. HKUST6148/03E. Thanks are also due to M. Hopfinger, W. P. Lee, C. T. Hsu, C.Y Tsoi and K. N. Leung for their help in the simulation parts of the paper.

REFERENCES

- [1] E. Fossum, "CMOS image sensors: Electronic camera-on-chip," *IEEE Transactions on Electron Devices*, Vol.44, No.10, 1997, pp.1689-1698.
- [2] F. Boussaid, A. Bermak and A. Bouzerdoun, "A wide dynamic range CMOS imager with extended shunting inhibition image processing capabilities," *IEEE International Symposium on Circuits and Systems, 2001. ISCAS 2001*, Vol. 3 , pp.620 - 623, 2001.
- [3] A. Bermak, F. Boussaid, and A. Bouzerdoun, "A CMOS imager with on-chip processing for image enhancement and edge detection," *Canadian Journal of Electrical and Computer Engineering*, vol. 26, no. 3-4, pp. 153-157, 2001.
- [4] Jorg Kramer, "An ON/OFF Transient Imager with Event-Driven, Asynchronous Read-out," *IEEE International Conference on Circuit and Systems, ISCAS02*, Vol.II, pp.165-168, USA, 2002.
- [5] A. J. Sutherland, A. Hamilton, D. A Renshaw, M. A. Glover, "Analogue VLSI For Temporal Frequency Analysis of Visual Data," *IEEE International Conference on Circuit and Systems, ISCAS02*, Vol.III, pp.743-746, USA, 2002.
- [6] E. Culurciello, R. Etienne-Cummings, and K. Boahen, "A biomorphic digital image sensor," *IEEE Journal of Solid-State Circuits*, Vol.38, No.2, 2003, pp.281-294.
- [7] S. R. Schultz and M. A. Jabri, "Analogue VLSI 'integrate and fire' neuron with frequency adaptation," *Electronic Letters*, Vol.31, No.16, 1995, pp.1357-1358.
- [8] K.A Boahen, "Retinomorphic Vision Systems: Reverse Engineering the Vertebrate Retina," *Ph.D. thesis, California Institute of Technology, Pasadena CA*,, 1997.
- [9] A. Van Schaik, "Building Blocks for electronic spiking neural networks," *Neural Networks*, Vol.14, No.6-7, 2001, pp.617-628.
- [10] W. Yang, "A wide-dynamic-range, low-power photosensor array," *ISSCC'94*, pp.230231, USA, San Francisco, Feb. 1994.
- [11] G. Indiveri "A Low-Power Adaptive Integrate-and-fire Neuron Circuit," *International Conference on Circuit and Systems, ISCAS03*, Vol.IV, pp.820-823, Thailand, 2003.
- [12] S. Campbell, D. Wang, and C. Jayaprakash, "Synchrony and Desynchrony in Integrate-and-Fire Oscillators", *Neural Computation*, no.11, pp.1595-1619, 1999.
- [13] H. Ando, *et al.* "A Nonlinear Oscillator Network Circuit for Image Segmentation with Double-threshold Phase Detection," *International Conference on Artificial Neural Network, ICANN99*, pp.655-660, 7-10, Sept. 1999.
- [14] Holst G. C., "CCD Arrays, Cameras and Displays," *SPIE Optical Engineering Press*, 1996.
- [15] G. B. Ermentrout, and N. Kopell "Parabolic Bursting in an Excitable System Coupled with a Slow Oscillation," *SIAM J. Applied Mathematics*, pp.233-253.
- [16] E. M. Izhikevich, "Class 1 Neural Excitability, Conventional Synapses, Weakly Connected Networks, and Mathematical Foundations of Pulse-Coupled Models," *IEEE Transactions on Neural Networks*, Vol.10, No.3, 1999, pp.499-507.
- [17] C. Von der Marlsburg, and W. Schneider "A Neural Cocktail-Party Processor," *Biol. Cybernetics*, 1986, pp.29-40.